Mon. Not. R. Astron. Soc. **000**, 000–000 (0000) Printed 4 March 2009 (MN LATEX style file v2.2)

Segue 2: A Prototype of the Population of Satellites of Satellites

V. Belokurov[1], M.G. Walker[1], N.W. Evans[1], G. Gilmore[1], M.J. Irwin[1], M. Mateo[2], L. Mayer[3], E. Olszewski[4], J. Bechtold[4], T. Pickering[5].

[1]*Institute of Astronomy, University of Cambridge, Madingley Road, Cambridge, CB3 0HA, UK*
[2]*Department of Astronomy, University of Michigan, Ann Arbor, MI 48109, USA*
[3]*Institute for Theoretical Physics, University of Zürich, CH-8057 Zürich, Switzerland*
[4]*Steward Observatory, University of Arizona, Tucson, AZ 85721, USA*
[5]*MMT Observatory, University of Arizona, Tucson, USA*

4 March 2009

ABSTRACT

We announce the discovery of a new Milky Way satellite Segue 2 found in the data of Sloan Extension for Galactic Understanding and Exploration (SEGUE). We followed this up with deeper imaging and spectroscopy on the Multiple Mirror Telescope (MMT). From this, we derive a luminosity of $M_v = -2.5$, a half-light radius of 34 pc and a systemic velocity of ~ -40 kms^{-1}. Our data also provides evidence for a stream around Segue 2 at a similar heliocentric velocity, and the SEGUE data show that it is also present in neighbouring fields. We resolve the velocity dispersion of Segue 2 as 3.4 kms^{-1} and the possible stream as ~ 7 kms^{-1}. This object shows points of comparison with other recent discoveries, Segue 1, Boo II and Coma. We speculate that all four objects may be representatives of a population of satellites of satellites – survivors of accretion events that destroyed their larger but less dense parents. They are likely to have formed at redshifts $z > 10$ and are good candidates for fossils of the reionization epoch.

Key words: galaxies: dwarf — galaxies: individual (Segue 2) — Local Group

1 INTRODUCTION

The idea that the outer parts of Galactic haloes are built up from the merging and accretion of satellites is now well-established. The building blocks that contributed most to the Galactic halo have been broken down into streams of debris. Reconstructing the history is difficult as the progenitors have been disassembled and phase mixed. In Cold Dark Matter cosmogonies, smaller haloes form earlier and are denser (Navarro et al. 1997). So, the entourage of the accreted progenitors, smaller satellites of the bigger satellites, may have survived against tidal destruction (see e.g., Diemand et al. 2008).

Amongst the recent discoveries of Milky Way satellites, there are objects whose properties are unlike conventional globular clusters or dwarf galaxies, such as Coma, Segue 1 and Boo II (Belokurov et al. 2007; Walsh et al. 2007). They have half-light radii of $\sim$ 30-70 pc and luminosities below $M_v = -3$. In fact, Coma, Segue 1 and Boo II lie projected on the Sagittarius stream, and have velocities consistent with Stream membership. Irrespective of whether they are dwarf galaxies or globular clusters, it seems reasonable to conclude that they once belonged to the Sagittarius galaxy. Could they be the first examples of a population of satellites of satellites?

In this Letter, we report the discovery of a further object analogous to Coma, Segue 1 and Boo II. Using the recently available SEGUE imaging, we have extended our ongoing survey of stellar overdensities in the outer Milky Way halo. We followed up the new object – called Segue 2 – with deep imaging and high resolution spectroscopy and present its properties and possible genealogy here.

2 DATA AND DISCOVERY

The original Sloan Digital Sky Survey (SDSS) imaged most of the North Galactic Cap plus three stripes of data in the South Galactic Cap (Abazajian et al. 2009). The SEGUE survey (Yanny et al. 2009) is primarily spectroscopic, but complements the SDSS imaging data with 15 2.5° wide stripes along constant Galactic longitude, spaced by approximately 20° around the sky. The stripes probe the Galaxy at a variety of longitudes, sampling the changing relative densities of thin disk, thick disk, and halo. The SEGUE imaging footprint is illustrated at `http://www.sdss.org/dr7/seguephoto_big.gif`

Figure 1 shows the familiar picture of the "Field of Streams" (Belokurov et al. 2006a), together with the SEGUE imaging stripes with right ascension $\alpha < 90°$ and declination $\delta < 50°$. We have also cut on Galactic latitude $b < -20°$ to avoid showing regions dominated by the Galactic disk. As is usual, the magnitudes of stars have been corrected for extinction using the maps

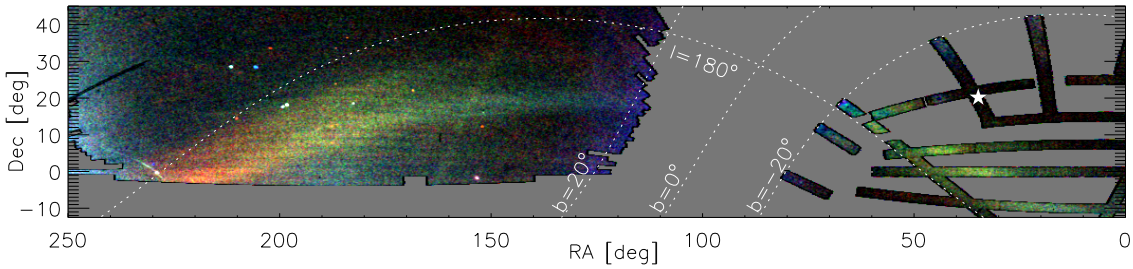

Figure 1. Location of Segue 2 marked by asterisk with respect to "the Field of Streams". in SEGUE imaging. This is a stellar density plot of all stars with $20.0 < i < 22.5$ and $-1 < g - i < 0.6$. The magnitude range is divided into three equal-sized bins analogous to Belokurov et al. (2006a). Note that the Sagittarius Stream trailing arm is clearly visible crossing the equator at right ascensions $\alpha \sim 40°$.

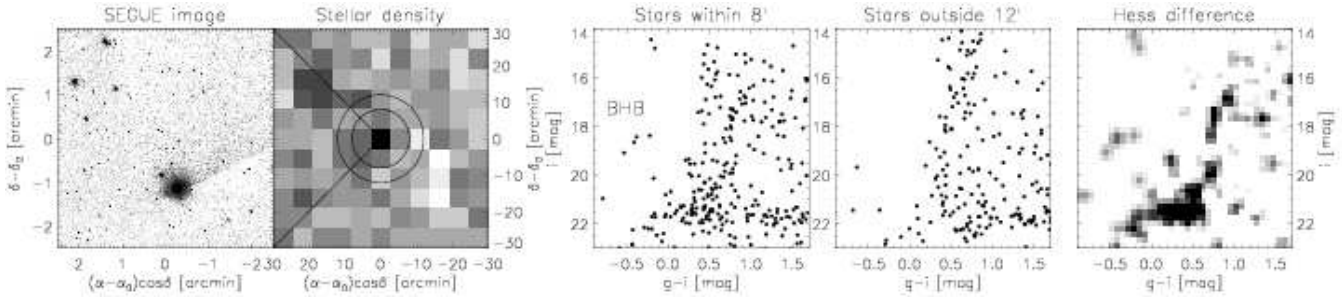

Figure 2. Leftmost two panels: SEGUE image of the $5' \times 5'$ field centered on Segue 2 and density of all objects classified as stars in a $30' \times 30'$ field. Note the bright saturated star and associated artefacts. The annuli are used in the construction of the CMDs. Rightmost three panels: CMD of the inner and outer regions, together with their Hess difference. There is a clear main sequence turn-off, together with sparse red giant branch (RGB) and blue horizontal branch (BHB).

of Schlegel et al. (1998). Running the algorithm for identification of overdensities described in Belokurov et al. (2006b), we isolate high significance peaks. The location of the highest is marked by a white asterisk in Figure 1.

Figure 2 shows the SEGUE view of the overdensity. The leftmost panel is a cut-out of the sky with the overdensity at the centre. The only discernible structure is in fact an unrelated saturated foreground star and accompanying artefacts. In the next panel, the density of resolved stars is shown, and now there is an evident overdensity with significance (Koposov et al. 2008) $S = 4.7$ at the centre of the image. Annuli are marked which are used to select stars within $8'$ and outside $12'$ for the two color magnitude diagrams (CMDs). The rightmost panel gives the Hess difference, and there is a clear main-sequence turn-off, together with definite hints of a red giant branch (RGB) and a blue horizontal branch (BHB).

Property	
Coordinates (J2000)	$\alpha = 02:19:16$, $\delta = 20:10:31$
Coordinates (Galactic)	$\ell = 149.4°$, $b = -38.1°$
$v_\odot$, σ	-39.2 ± 2.5, $3.4^{+2.5}_{-1.2}$ kms^{-1}
Position Angle	$182° \pm 17°$
Ellipticity	0.15 ± 0.1
r_h (Exponential)	$3.'4 \pm 0.'2$
$(m-M)_0$	$17.^m7 \pm 0.^m1$
$M_{tot,V}$	$-2.^m5 \pm 0.^m2$

Table 1. Properties of the Segue 2 Satellite

3 FOLLOW-UP

3.1 Imaging

Follow-up imaging of Segue 2 was carried out on Oct 7 2007 using the Megacam imager (Mcleod et al 2006) on the Multiple Mirror Telescope (MMT). Megacam comprises 36 2048x4608 E2V CCDS. With 2x2 binning, pixels are $0.16''$ and each image is $24' \times 24'$ in size. Six 300s exposure images in r' and 7 in g' were collected with dithers of 100-200 pixels in each coordinate between frames. Frames were processed using SAO's MEGARED package and combined using SWARP package in TERAPIX (Radovich et al. 2001). A final set of object catalogs was generated from the stacked images and objects were morphologically classified as stellar or non-stellar (or noise-like). The detected objects in each passband were then merged by positional coincidence (within $1''$) to form a combined g, r catalogue and photometrically calibrated on the SDSS system using stars in common.

Figure 3 compares the original SEGUE data with the Megacam follow-up. From the CMDs, it is immediately clear that the Megacam data probe at least 2 magnitudes deeper and reveal the main sequence of Segue 2 . The algorithm of Martin et al. (2008) is applied to stars selected by the masks shown in the Figure. Model isodensity contours, based on both the SEGUE and Megacam data, are shown in the lower panels. We see that the shallower SEGUE data yields a slightly more extended and elliptical light profile. The extracted structural parameters using the deeper Megacam data are listed in Table 1. There are possibly 4 BHB stars associated with Segue 2 , which can be used to obtain a distance modulus $m - M = 17.7$ or 35 kpc. Using this, the half-light radius is $r_h = 34$ pc which is small compared to typical ultrafaint dwarf galaxies (Belokurov et al. 2007; Gilmore et al. 2007).

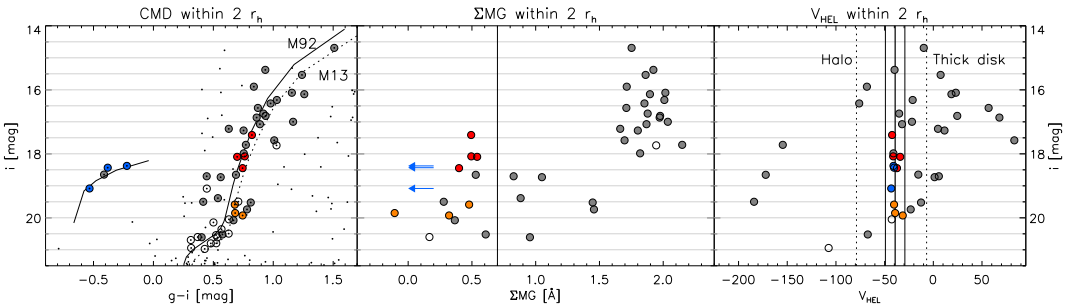

Figure 4. Left: CMD of all stars (black dots) within $2r_h$, with objects followed-up spectroscopically circled. Filled circles with valid velocities and ΣMg color-coded such that gray shows the foreground population, red shows red clump giants, blue show BHBs and orange subgaints in Segue 2 . The M92 ridgeline (including the BHB) is overplotted together with the M13 ridgeline for comparison. Middle: The distribution of ΣMg values, showing clean separation between dwarfs in the thick disk (high ΣMg) and giants in Segue 2 (low ΣMg) at bright magnitudes. The vertical solid line marks the boundary adopted here. Note that at fainter magnitudes, there is a population of stars with intermediate ΣMg and velocities similar to the systemic velocity of Segue 2 . Right: Heliocentric radial velocities of all stars with good spectra. The characteristic velocities associated with the halo and thick disk at this location are enclosed by vertical dashed lines, together with solid lines showing the systemic velocity of Segue 2 plus or minus 10 kms^{-1}.

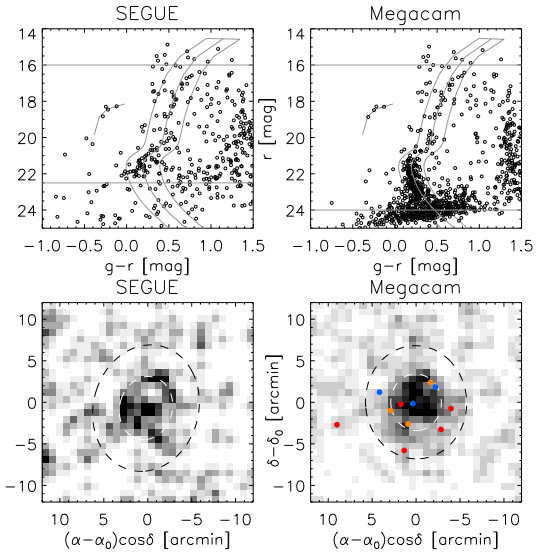

Figure 3. Top left and right; CMDs of Segue 2 in SEGUE and in the follow-up Megacam data, which goes at least 2 mag deeper. The follow-up data shows a well-defined main sequence, with grey lines marking the ridgeline of M92 and the mask used to select members. Bottom left and right: Grey-scale density of stars selected by in the 24′ × 24′ field of view centered on Segue 2 . The ellipses show the model isodensity contours corresponding to r_h and $2r_h$. The colored dots show the locations of likely members followed up spectroscopically.

3.2 Spectroscopy

On 22-23 and 26 October 2008, we obtained high resolution spectra of 358 targets around Segue 2 using three independent fiber configurations with the Hectochelle spectrograph at the MMT. Over the 1° field, we targeted RGB candidates as faint as $i \sim 21.5$, as well as the handful of BHB candidates at $i \sim 18.5$. We extracted and calibrated spectra following the procedure described by Mateo et al. (2008). The Hectochelle spectra span 5150−5300 Å, where RGBs and foreground dwarfs prominently exhibit the Mg-I/Mg-b triplet (MgT) absorption feature. For the RGB candidates, we measure velocity by cross-correlating each spectrum against a high signal-to-noise template spectrum, built from co-added spectra of late-type radial velocity standards observed with Hectochelle. However, this template poorly resembles the spectrum of a BHB, in which high temperature suppresses Mg absorption and the only prominent absorption feature is the FeI/FeII blend at 5169 Å. Thus, for each BHB candidate, we measure the centroid of this feature and calculate velocity directly from the redshift. For all spectra, we also measure a composite magnesium index, ΣMg, effectively a pseudo-equivalent width for the MgT (Walker et al. 2007). This quantity correlates with metallicity, temperature and surface gravity, and helps to separate members from foreground. We determine measurement errors for both velocity and ΣMg using the bootstrap method described by Walker et al. (2009). Velocities and ΣMg in the Segue 2 sample have mean (median) errors of 1.1 (0.6) km s^{-1} and 0.20 (0.17) Å , respectively.

Figure 4 shows correlations between the photometric and spectroscopic properties of stars within $2r_h$. The first panel shows the locations of stars targeted for follow-up on the CMD, together with the ridgelines of M92 ([Fe/H] = -2.24) and M13 ([Fe/H] = -1.65) from Clem et al. (2008). The second and third panels show ΣMg and v_{HEL} plotted against i band magnitude, from which we will identify three classes of Segue 2 members, namely bright red clump giants (RCGs), fainter RGBs and BHBs, and two types of contaminants, Galactic foreground and possible tidal stream.

One population clearly stands out in the ΣMg panel. Given the magnitude distributions, it is evident that the stars with higher ΣMg are dwarfs in the Galactic thick disk. At a similar magnitude $i \sim 17.5$, there is only one other population with a tight ΣMg distribution, namely the red clump stars visible in the first panel. These form a narrow distribution in velocity space, suggesting that the systemic velocity is ~ -40 kms^{-1}. Sample spectra of a Galactic dwarf and a RCG are shown in Figure 5. Note that the dwarf has higher surface gravity and potentially higher metallicity than the RCGs, and hence has broader absorption features. The velocity signature is corroborated by the three BHBs, which all have velocities ~ -40 kms^{-1}. Finally, we use the systemic velocity of Segue 2 with a range of ±10 kms^{-1} as a secondary cut, as shown by the vertical lines in the third panel. This gives a further three candidate members (shown in yellow), which all lie redwards of the M92 ridgeline and are better described by more metal-rich templates like M13. An example of their spectra is illustrated in the fourth panel of Figure 5. Unfortunately, the low signal-to-noise does not allow the direct extraction of the metallicity for these stars.

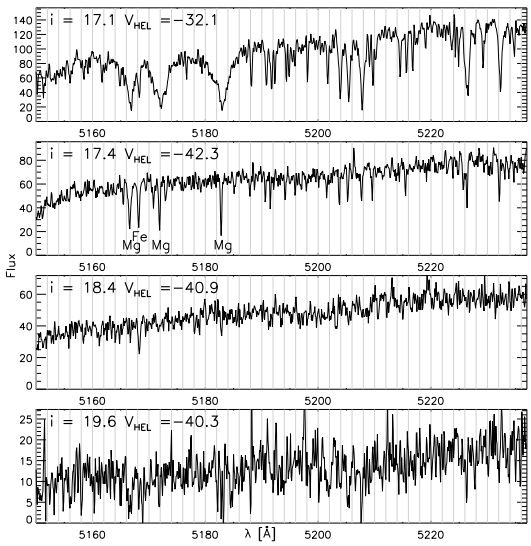

Figure 5. Examples of spectra of thick disk contaminant (top), together with three members of Segue 2 , a RCG (upper middle), a BHB (lower middle) and a faint RGB (bottom). Only the bluer part of the wavelength range containing the MgT is shown.

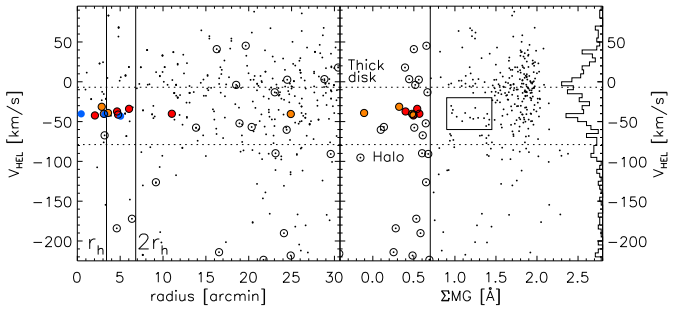

Figure 6. Heliocentric radial velocity versus elliptical radius (left) and ΣMg (right). All the stars with measured ΣMg are shown as black dots, whilst stars satisfying ΣMg < 0.7 are circled. The extent of Segue 2 is illustrated by the vertical lines showing r_h and $2r_h$. The open circled stars do not appear to be kinematically associated with Segue 2 . The structural parameters inferred from the photometry are consistent with the spectroscopic and kinematic signal. Note that the velocity histogram on the extreme right reveals a substantial population of stars with $-60 < v_{HEL} < -30$ kms^{-1} that cannot be attributed to either thick disk or halo.

These three fainter giant stars may be representatives of a distinct population with low to intermediate ΣMg , clearly visible in the second panel. The velocities of the stars in this population are offset from the thick disk, but roughly centered on Segue 2 . The population is much more evident in Figure 6, which shows all stars with measured velocities and ΣMg within 45′. The velocity histogram along the rightmost vertical of the plot shows that the foreground consists of the expected thick disk and halo populations, together with an unknown component, perhaps a tidal stream. The stars in this component extend over the entire field and they are kinematically colder than the thick disk but significantly hotter than Segue 2 .

The left panel of Figure 7 shows the SEGUE spectroscopic footprint around Segue 2 . The right panel shows the distributions of radial velocities corrected to the Galactic Standard of

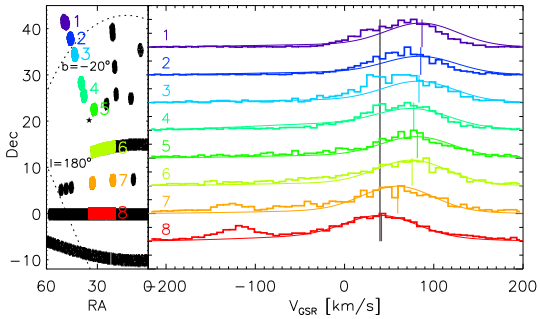

Figure 7. Left: SEGUE spectroscopic fooprint in the vicinity of Segue 2 . Right: Histograms of radial velocities corrected to the Galactic Standard of Rest in fields coded according to color. The black vertical lines shows the systemic velocity of Segue 2 , whilst the colored ones show the mean velocity of the thick disk. The smooth curves show the sums of Gaussian velocity distributions of thick disk ($\langle v\rangle = 180, \sigma = 50$ kms^{-1}) and halo ($\langle v\rangle = 0, \sigma = 100$ kms^{-1}). Note the prominent bumps in the red and orange histograms corresponding to the Sagittarius trailing arm, and similarly the bumps in the pale blue and green histograms.

Rest are shown for each color-coded field. The underlying smooth curves come from a simple model of the Galactic thick disk and halo represented as two Gaussians with means and dispersions of ($\langle v\rangle = 180, \sigma = 50$ kms^{-1}) and ($\langle v\rangle = 0, \sigma = 100$ kms^{-1}) respectively. We immediately notice the presence of bumps or cold features in several fields. At low declination, the Sagittarius trailing arm is detected at $v_{GSR} \approx -120$ kms^{-1}. At higher declinations, there are significant deviations from the smooth curves at velocities $v_{GSR} \approx 40$ kms^{-1}, which is close to the systemic velocity of Segue 2 .

More speculatively, we suggest that the stream-like overdensity seen in the MMT data is part of the same structure as the features seen in the velocity histograms in the higher declination (lower Galactic latitude) SEGUE fields. This could be confirmed with distance estimates to the structures. There are many possibilities as to the nature of this overdensity. First, it could be part of the Sagittarius Stream, which lies in the same area of the Sky. However, the bulk of the Sagittarius debris lies at a lower declination (see Figure 1). Another possibility is the Monoceros ring (Yanny et al. 2003), visible in the SDSS data at the same Galactic longitude but positive latitude. However, the kinematic feature in the SEGUE fields seems too localized and is limited to latitudes $-30° < b < -20°$. Finally, (Majewski et al. 2004) reported the detection of an extended structure – perhaps a segment of tidal debris – a few degrees away from these fields as part of their survey of the Andromeda galaxy. Irrespective of which possibility is correct, our hypothesis is that Segue 2 is embedded in a tidal stream.

4 PHYSICAL PROPERTIES AND STELLAR POPULATION

Assuming Segue 2 has a Gaussian velocity distribution, we measure its velocity dispersion using a maximum-likelihood method. Specifically, we evaluate the marginal likelihood obtained after integrating the usual Gaussian likelihood over all mean velocities (see Equations 1 and 2 of Kleyna et al. (2004)). We find the velocity dispersion that maximizes this likelihood and determine the boundaries that enclose 68% and 95% of the area under the likelihood curve. For the five bright RCGs (marked in red in Fig. 6), we measure a velocity dispersion $\sigma_{V_0} = 3.4^{+2.5(+8.2)}_{-1.2(-2.2)}$ km s^{-1}. This result is

not strongly sensitive to our membership criteria – if we include the three fainter candidates (orange points in the Figures) passing our initial velocity and magnesium cuts we obtain $\sigma_{V_0} = 3.6^{+1.7(+4.5)}_{-1.0(-2.3)}$ km s^{-1}.

Our analysis indicates that we resolve the central velocity dispersion of Segue 2 , ruling out zero with more than 99% confidence. Adopting the idealised assumptions of spherical symmetry, dynamical equilibrium and "mass follows light," implicit in the formula $M = 850 r_h \sigma^2_{V_0}$ (Illingworth 1976; Simon & Geha 2007), the velocity dispersion of the five bright RCG members implies a dynamical mass of $M = 5.5^{+10.9(+52)}_{-3.1(-4.3)} \times 10^5 M_\odot$, and a mass-to-light ratio of $M/L_V = 650^{+1300(+6200)}_{-380(-520)} [M/L_V]_\odot$.

We can also estimate the kinematic properties of the stream from 15 prospective stream members satisfying $-60 \leq V \leq -20$ km s^{-1} and $0.9 \leq \Sigma\mathrm{Mg} \leq 1.45$ shown as a box in Figure 6. The mean velocity of the stream is $-45.1 \pm 0.1(\pm 0.2)$ kms^{-1} with 1 σ (2 σ) errors. This is obtained by marginalizing over the dispersion. It is offset by ~ 5 kms^{-1} from the systemic velocity of Segue 2 . The velocity dispersion of the stream is $7.1^{+1.8(+4.2)}_{-1.2(-2.1)}$ kms^{-1}.

For the brightest members of Segue 2 (the BHB and RCG stars), the signal-to-noise of the spectra is good enough to estimate metallicity. This was done by directly comparing the average continuum normalised spectrum of the three BHB spectra satisfying $18.0 < g < 19.0$ and the average of the five best RCG spectra satisfying $18.0 < g < 19.2$, with a grid of model atmosphere spectra (see Walker et al. (2009) for further details). Using the relationship $\log_{10}(T_{\rm eff}) = 3.877 - 0.26(g-r)$ (Ivezić et al. 2006), the average color ($\langle g-r \rangle = 0.53$) of the five RCG members implies $\langle T_{\rm eff} \rangle = 5500$K for these stars, while for the BHB stars the average color ($\langle g-r \rangle = -0.22$) implies $\langle T_{\rm eff} \rangle = 8600$K. Anchoring the $T_{\rm eff}$ for the spectral fit tightens constraints on gravity and metallicity, giving $\log g = 2.5 \pm 0.5$ and [Fe/H] $= -2.0 \pm 0.25$ for the averaged BHB stars and $\log g = 2.5 \pm 0.5$ and [Fe/H] $= -2.0 \pm 0.25$ for the averaged RCG stars. For the latter, each had sufficiently strong Mg and Fe lines and continuum signal-to-noise to model individually. In all cases the best fit model spectrum satisified $2.0 \leq \log g \leq 3.0$; 5000K $\leq$ T$_{\rm eff}$ $\leq$ 5500K and $-2.5 \leq$[Fe/H]≤ -2.0 corroborating their categorisation as RCG stars. These colors, magnitudes, surface gravities and effective temperatures are all fully consistent with the BHB and RCG stars being at a common distance (see, e.g., Gray 2005, p. 57).

5 CONCLUSIONS

A search in the high Galactic latitude ($|b| > 20^\circ$) area covered by SEGUE imaging has revealed another new satellite. Segue 2 has a half-light radius of ~ 30 pc and an absolute magnitude of $M_v = -2.5$. The photometry and spectroscopy suggest that the metallicity [Fe/H] ~ -2. Segue 2 is similar in structure, size, luminosity and velocity dispersion to three other recent discoveries, namely Segue 1, Boo II and Coma.

The latter three are likely to be embedded in the Sagittarius Stream. For example, Coma is superposed on the edge of the Stream and is at a distance that suggests association with the old leading (C) arm of the Sagittarius. Niederste-Ostholt et al. (2009) shows that Segue 1 stars are indistinguishable from the Sagittarius Stream, both photometrically and kinematically. It is natural to conclude that Segue 1 was once a satellite of the Sagittarius galaxy. Koch et al. (2009) have shown that Boo II lies close to the young leading (A) and old trailing (B) arms of the Sagittarius, and has similar kinematics.

There is indirect evidence that our new discovery Segue 2 is also immersed in a stream. To begin with, it lies on the edge of the Sagittarius stream, as seen by the SEGUE survey. Kinematically, there is a cold stream-like component in both our follow-up spectroscopy and in the SEGUE spectroscopy of nearby fields.

We speculate that all four objects are possibly satellites of satellites, remnants from the disruption of larger galaxies in the Milky Way halo. Under the simple assumption of an isothermal halo, the current circular velocity of Segue 2 is $v_{\rm circ} \sim 5$ kms^{-1}. The original $v_{\rm circ}$ before the tiny dwarf accreted onto the Milky Way halo as part of a parent subgroup might have been close to $10-15$ kms^{-1} (a reducton by a factor of $2-3$ is expected as a result of tidal shocks – see Mayer et al. 2007). Initial halo masses corresponding to such circular velocities are below $10^7 M_\odot$. With such low masses, these satellites of satellites are likely to have formed before reionization, at $z > 10$, since afterwards gas would have been photoevaporated owing to heating by the cosmic ionizing background (Barkana & Loeb 1999). Such an early formation epoch would naturally imply a high central density and a resulting resilience to tidal disruption of their inner core. The inner, surviving core of the object is what we may be witnessing in these four objects. These, and not the more luminous, ordinary dwarf spheroidal satellites of the Milky Way and M31, are good candidates for being fossils of the reionization epoch (Diemand et al. 2007). Accounting properly for their origin in the context of the formation of the Local Group is crucial in order to interpret correctly the discrepancy between the observed luminosity function of satellites and the predicted substructure mass function. Satellites of satellites are only resolved in the most recent dark matter cosmological simulations of the Milky Way halo (Diemand et al. 2008), but not yet in more realistic fully hydrodynamical simulations that account for the various mechanisms to which baryons are subject. Being able to identify satellites of satellites in cosmological hydrodynamical simulations will thus be a crucial step for interpreting new observations such as those presented here.

ACKNOWLEDGEMENTS

Funding for the SDSS and SDSS-II has been provided by the Alfred P. Sloan Foundation, the Participating Institutions, the National Science Foundation, the U.S. Department of Energy, the National Aeronautics and Space Administration, the Japanese Monbukagakusho, the Max Planck Society, and the Higher Education Funding Council for England. The SDSS Web Site is http://www.sdss.org/. Some of the observations reported here were obtained at the MMT Observatory, a joint facility of the Smithsonian Institution and the University of Arizona.

This work is based (in part) on data products produced at the TERAPIX data center located at the Institut d'Astrophysique de Paris. MM acknowledges support from NSF grants AST-0206081 0507453, and 0808043. EO acknowledges support from NSF Grants AST-0205790, 0505711, and 0807498.

REFERENCES

Abazajian, K. N. et al. 2009, ApSS, in press
Barkana, R., & Loeb, A. 1999, ApJ, 523, 54
Belokurov, V., et al. 2006a, ApJL, 642, L137
Belokurov, V., et al. 2006b, ApJL, 647, L111
Belokurov, V., et al. 2007, ApJ, 654, 897

Clem, J. L., Vanden Berg, D. A., & Stetson, P. B. 2008, AJ, 135, 682
Diemand, J., Kuhlen, M., & Madau, P. 2007, ApJ, 667, 859
Diemand, J., Kuhlen, M., Madau, P., Zemp, M., Moore, B., Potter, D., & Stadel, J. 2008, Nature, 454, 735
Gilmore, G., Wilkinson, M. I., Wyse, R. F. G., Kleyna, J. T., Koch, A., Evans, N. W., & Grebel, E. K. 2007, ApJ, 663, 948
Gray, D. F. 2005, The Observation and Analysis of Stellar Photospheres (Cambridge University Press)
Illingworth, G. 1976, ApJ, 204, 73
Ivezić, Z. et al. 2006, Memorie della Societa Astronomica Italiana, 77, 10 57
Kleyna, J. T., Wilkinson, M. I., Evans, N. W., & Gilmore, G. 2004, MNRAS, 354, L66
Koch, A., et al. 2009, ApJ, 690, 453
Koposov, S., et al. 2008, ApJ, 686, 279
Majewski, S. R., Ostheimer, J. C., Rocha-Pinto, H. J., Patterson, R. J., Guhathakurta, P., & Reitzel, D. 2004, ApJ, 615, 738
Martin, N. F., de Jong, J. T. A., & Rix, H.-W. 2008, ApJ, 684, 1075
Mateo, M., Olszewski, E. W., & Walker, M. G. 2008, ApJ, 675, 201
Mayer, L., Kazantzidis, S., Mastropietro, C., & Wadsley, J. 2007, Nature, 445, 738
McLeod, B., Geary, J., Ordway, M., Amato, S., Conroy, M., & Gauron, T. 2006, Scientific Detectors for Astronomy 2005, 337
Navarro, J. F., Frenk, C. S., & White, S. D. M. 1997, ApJ, 490, 493
Niederste-Ostholt, M. et al. 2009, MNRAS, submitted
Radovich, M., Mellier, Y., Bertin, E., Missonnier, G., Didelon, P., Morin, B., Dantel-Fort, M., & McCracken, H. 2001, Mining the Sky, 554
Schlegel, D. J., Finkbeiner, D. P., & Davis, M. 1998, ApJ, 500, 525
Simon, J. D., & Geha, M. 2007, ApJ, 670, 313
Walker, M. G., Mateo, M., Olszewski, E. W., Bernstein, R., Sen, B., & Woodroofe, M. 2007, ApJS, 171, 389
Walker, M., et al. 2009, ApJL, submitted
Walsh, S. M., Jerjen, H., & Willman, B. 2007, ApJL, 662, L83
Yanny, B., et al. 2003, ApJ, 588, 824
Yanny, B. 2009, ApJ, in press